16TH EUROPEAN CONFERENCE ON EARTHQUAKE ENGINEERING THESSALONIKI 18 - 21 JUNE 2018

MACRO-MODEL FOR RIGID PILE FOUNDATION IN COHESIVE-FRICTIONAL SOILS: DETERMINATION OF THE FAILURE SURFACE

Noussaiba GRAINE[1], Mohammed HJIAJ[2], Kristian KRABBENHOFT[3]

ABSTRACT

A key component in describing the dissipative behaviour of the soil-pile system in macro-element models for soil-structure interaction is the definition of the plastic constitutive governing equations. In particular, the failure surface plays a critical role in such modelling owning the complex interaction between the pile and the soil mass. The purpose of this paper is to construct the failure surface for a single rigid pile in a cohesive-frictional soil, subjected to both horizontal force and bending moment. Accurate upper and lower bounds to the failure loads of a rigid pile embedded in homogeneous cohesive-frictional soil are computed numerically via the novel limit analysis software OPTUM^{G3}. The results are presented in the form of a normalized failure surface in *M-H* plane with an error ranging between 3% and 10%. An estimation of the exact collapse loads by means of mixed elements is provided additionally. A parametric study investigate the influence of the problem parameters on the ultimate loads. A closed form expression of the failure surface is derived and calibrated with the numerical results.

Keywords: Macro-element; Soil-structure-interaction; Pile foundations; Failure surface

1. INTRODUCTION

In the field of earthquake engineering, soil-structure interaction (SSI) is an important phenomenon that has to be taken into account to reproduce correctly the non-linear behaviour of a structure and therefrom be able to predict its relative displacements. Piled foundations are commonly used to resist dynamic lateral loads either transient or repetitive. The prediction of its response to horizontal, time dependent loadings such as caused by earthquakes is a challenging problem in geotechnical engineering due to the complex interaction between the pile and the soil mass. Several methods have been proposed in the literature (Pecker 2015, Finn et al. 2010, Taciroglu et al. 2010, Correia 2011…) among which the macro-element technique that has received more and more attention in the recent years.

The concept of the macro-element (ME) aims at condensing the entire behaviour of the foundation-supporting soil system into a single element divided into two parts, one for the far field and the other for the near field. The far field (FF) corresponds to the zone of propagation of seismic waves modelled using dynamic impedances. The near field (NF) zone corresponds to a finite domain where all the nonlinearities occurring in the system are located. For the case studied, it includes both geometrical non-linearity that is contact interactions for pile foundations, and material non-linearity: plasticity of soil under the foundation or along the pile shaft as explained in Figure 1.

The response of the macro-element is described in terms of generalized forces versus generalized displacements, therefore allowing considerable decrease in the necessary degrees of freedom of the numerical model. The translational and rotational degrees of freedom of a macro-element are all fully coupled in the plastic range. This joint element is normally placed at the base of the superstructure. In case of shallow footings, it is located at the centre of mass of the foundation, while for deep foundations the joint element is positioned at the centre of the pile-head (Correia. 2011, Li.2016).

[1]PhD candidate, Institut National des sciences appliquées de Rennes, FRANCE, noussaiba.graine@insa-rennes.fr
[2]Professor, Institut National des sciences appliquées de Rennes, FRANCE, Mohammed.Hjiaj@insa-rennes.fr
[3]Professor, University of Liverpool, UK, Kristian.Krabbenhoft@liverpool.ac.uk

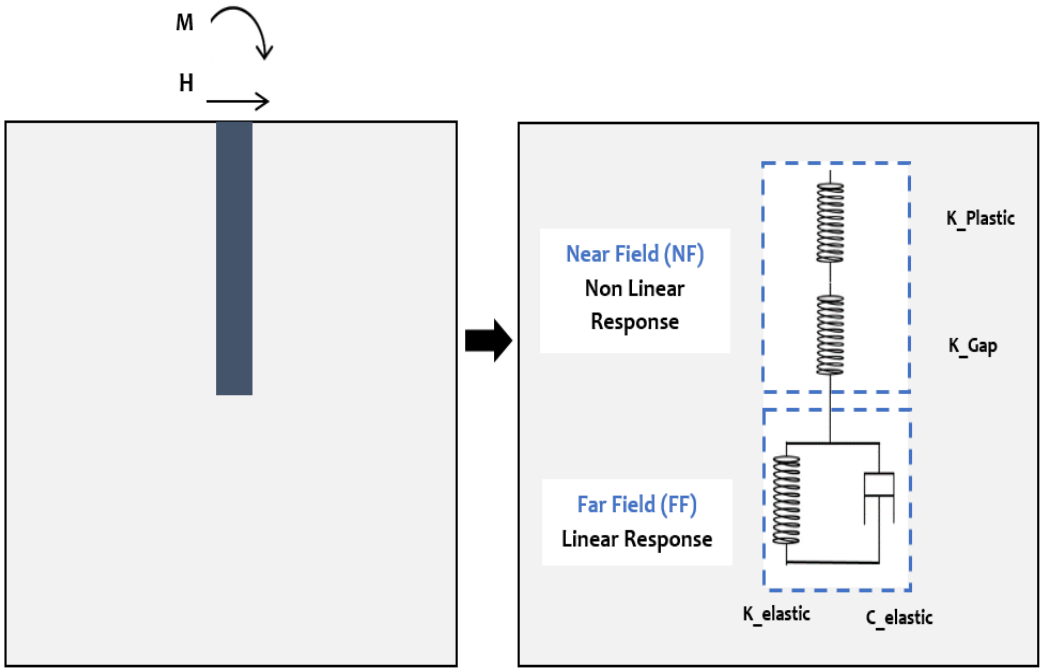

Figure 1: Pile-head macro-element concept

The process for the development of a macro-element model for soil-structure interaction starts with the definition of the initial elastic response by means of pile-head impedances; the ultimate collapse state is then determined by a suitable failure surface which describes all possible loading combinations that will induce failure of the foundation. Next, the plastic flow rule relating the incremental plastic displacements of the foundations to its limit loading surface and an adequate hardening rule is to be defined. In case of cyclic loading, a loading reloading rule is to be specified. In order to take into account the gap formation mechanism, a gap evolution model should be constructed additionally. This paper presents the preliminary results from the macro-element development process, which concern the definition of the ultimate surface of the "plasticity-type" model for the single pile foundation under lateral loading.
The rest is organized as follows. Section 2 defines the problem under consideration and introduces the notation used. Section 3 recalls the limit analysis theorems and presents the numerical model features. Numerical results are given in section 4. In section 5, the effects of soil friction angle, cohesion and unit weight as well as pile length to diameter ratio on the shape of the failure surface are discussed and a closed form expression is proposed for the yield surface. The paper ends with conclusions.

2. PROBLEM DEFINITION

The present study deals with a circular pile of length L and diameter D embedded into a deep homogeneous cohesive-frictional soil of great depth layer that is subjected to both a horizontal force H and a bending moment M (Figure 2). Further, it is assumed that the pile is rough and the soil is of unit weight γ. The pile head is at the ground surface level (i.e.: no eccentricity). The cohesive-frictional soil is assumed to be rigid perfectly plastic and modelled by the Mohr-Coulomb constitutive model. Tables 1a and 1b present the main parameters for the pile and the soil mass.
The limit load problem consists in finding the collapse multiplier, μ, the stress field and the velocity field such that governing equations of continuum mechanics are satisfied. The sign conventions for the pile head loads adopted in this paper are shown in Figure 3 which complies with the right handed axes and clockwise positive convention. The lateral capacities for pure loadings are denoted H_0 (when $M = 0$) and M_0 (when $H = 0$).

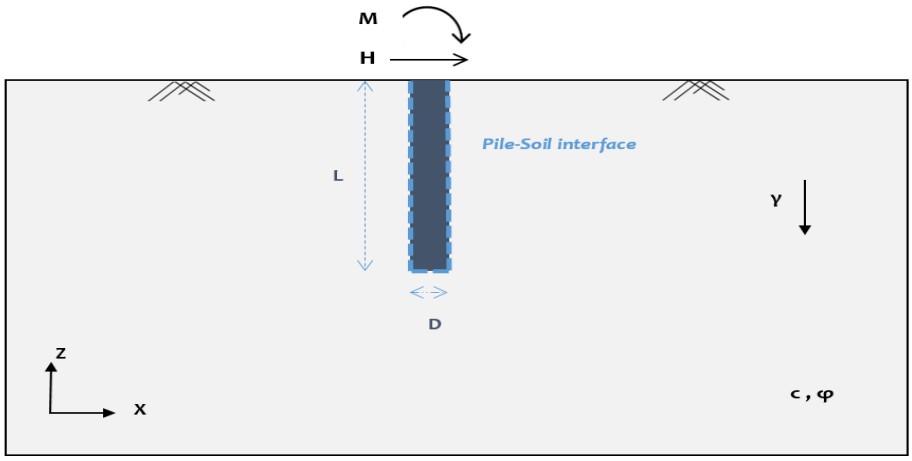

Figure 2. Single vertical free-headed pile under lateral loading

Table 1a. Soil Parameters.

Unit weight γ	Young's modulus E	Poisson's Ratio ν	Cohesion c	Friction angle φ
20 kN/m^3	40 MPa	0,3	10 kN/m^2	30°

Table 1b. Pile Parameters.

Unit weight γ_p	Pile length L	Pile diameter D
20 kN/m^3	5 m	1 m

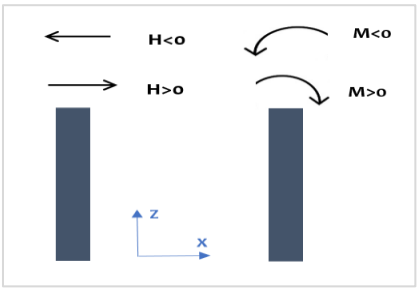

Figure 3. Sign conventions for pile head loading

3. NUMERICAL LIMIT ANALYSIS

The fundamental theorems of limit analysis define convex mathematical programs. After discretization, they can be solved by mathematical programming techniques. A full description of the present formulations can be found in (Lyamin et al. 2001, Lyamin et al. 2002).

3.1 Discrete formulation of the lower bound

In the lower bound formulation, the stress field is discretized using the finite elements with stress nodal variables, $\sigma(\mathbf{x}) = \mathrm{N}_i(\mathbf{x})\sigma_i$ where σ_i is a nodal stress vector and $\mathrm{N}_i(\mathbf{x})$ are shape functions, Figure 4. For a rigorous lower bound, the shape function must be linear to ensure that the yield criterion can be satisfied everywhere by enforcing it only at the nodal points of each element. Linear equality constraints on the nodal stresses arise from the application of equilibrium equations over each element. Equilibrium of the surface tractions emerging on both sides of adjacent triangles should also be enforced. Since the

shape functions are linear, this condition is satisfied by only matching traction components at nodal pairs that have the same coordinates and share the same edge. In addition to the above constraints, equilibrium equations on the boundary generate extra linear equalities that have to be added to the previous ones. The nonlinear constraints in the formulation arise from satisfaction of the yield criterion, which is implemented in its native form. The objective function of this nonlinear linear programming problem, which corresponds to the collapse load, is maximized according to:

$$\begin{aligned} &\textit{maximize} \quad \mathbf{C}^{\mathbf{T}}\boldsymbol{\Sigma} \\ &\textit{Subject to} \quad \begin{cases} \mathbf{A}\,\boldsymbol{\Sigma} = \mathbf{b} \\ f_i(\boldsymbol{\sigma}) \le 0 \quad i = \{1,...,n\} \end{cases} \end{aligned} \tag{1}$$

where $\mathbf{C}$ is a vector of objective function coefficients, $\boldsymbol{\Sigma}$ is a vector of unknowns (nodal stresses), $\mathbf{C}^{\mathbf{T}}\boldsymbol{\Sigma}$ is the collapse load, $\mathbf{A}$ is a matrix of equality constraint coefficients, $\mathbf{b}$ is a vector of coefficients, f_i is the yield function for node i, and n is the number of nodes.

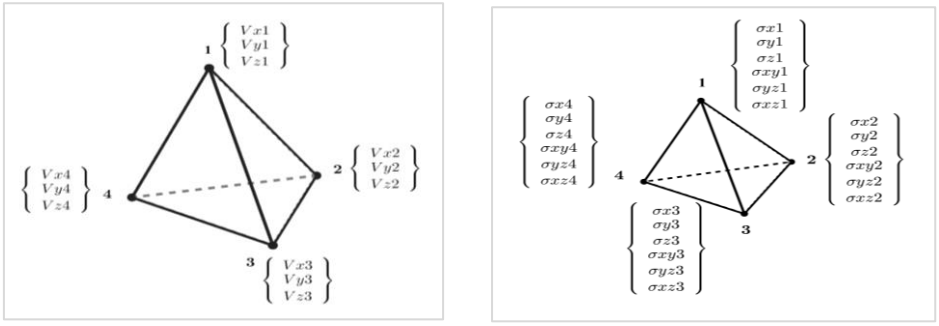

Figure 4 .3D upper and lower bound finite elements

3.2 Discrete formulation of the upper bound

The minimum principle arising from the upper bound theorem is cast in discrete form by expressing the velocity field as function of a finite number of parameters. Three dimensional finite elements based on velocity approximations are employed for this purpose. In each element $E\left(E = 1,....,N\right)$ the velocities are expressed as $\mathbf{v}(\mathbf{x}) = \mathrm{N}_i(\mathbf{x})\mathbf{v}_i$ where $\mathbf{v}_i$ is a nodal velocity vector and N_i are shape functions. The linear four-nodded element can be used to model the velocity field, Figure 4. This ensures that the upper bound is strict since the flow rule is satisfied everywhere within each element. Two unknown velocities are associated with each node, and a single plastic multiplier rate plus a constant stress vector are associated with each element. To improve the upper bound calculations and avoid locking that may occur for incompressible materials, velocity discontinuities are allowed (Sloan and Kleeman (1995)) along all shared element in the mesh. In their procedure, the direction of shearing is chosen automatically during the minimization process to give the least amount of dissipated power.

To avoid the Kuhn-Tucker constraints, the minimum problem can be transformed into a min-max problem. As a result of this transformation, the plastic multiplier rate does not appear explicitly in the formulation. Once the constraints and the objective function coefficient are assembled, the task of finding a kinematically admissible velocity field, which minimizes the internal power dissipation for a specified set of boundary conditions, may be written as:

$$\begin{aligned} &\underset{\boldsymbol{\Sigma}}{\textit{maximize}}\ \underset{\mathbf{V,d}}{\textit{minimize}}\ \ \boldsymbol{\Sigma}^{\mathrm{T}}\mathbf{B}\mathbf{V} + \mathbf{C}_{\mathrm{u}}^{\mathrm{T}}\mathbf{V} + \mathbf{C}_{\mathrm{d}}^{\mathrm{T}}\mathbf{D} \\ &\textit{Subject to} \quad \begin{cases} \mathbf{A}_{\mathrm{u}}\mathbf{V} + \mathbf{A}_{\mathrm{d}}\mathbf{D} = \mathbf{b} \\ f_i(\boldsymbol{\sigma}) \le 0 \quad \mathrm{i} = \{1,...,\mathrm{N}\} \\ \mathbf{D} \ge 0 \end{cases} \end{aligned} \tag{2}$$

where $\mathbf{V}$ is a global vector of unknown velocities, $\mathbf{D}$ is a global vector of unknown discontinuity variables, $\boldsymbol{\Sigma}$ is a global vector of unknown element stresses, $\mathbf{C}_u$ and $\mathbf{C}_d$ are vectors of objective function coefficients for the nodal velocities and discontinuity variables, $\mathbf{A}_u$ and $\mathbf{A}_d$ are matrices of equality constraint coefficients for the nodal velocities and discontinuity variables, $\mathbf{B}$ is a global matrix of compatibility coefficients that operate on the nodal velocities, $\mathbf{b}$ is a vector of coefficients, f_i is the yield function for element i, and N is the number of triangular elements. The objective function $\boldsymbol{\Sigma}^T\mathbf{B}\mathbf{V} + \mathbf{C}_u^T\mathbf{V} + \mathbf{C}_d^T\mathbf{D}$ corresponds to the total dissipated power, with the first term giving the dissipation in the continuum, the second term giving the dissipation due to fixed boundary tractions or body forces, and the third term giving the dissipation in the discontinuities.

3.3 OPTUM^{G3}: A new and powerful limit analysis software

OPTUM^{G3} is a novel and unique 3D comprehensive finite element program for geotechnical stability and deformation analysis. It is developed by Optum Computational Engineering, *OptumCE*. The code is an extension of an already well acknowledged finite element software OPTUM^{G2} for two dimensional analysis. Both robust yet very user friendly, they enable straightforward limit analysis computations. One of their striking features are automative adaptive mesh refinement, integrated preliminary analyses (initial stresses…) and a large material library. More details can be found in OptumCE (2015).

In the rest of the paper, accurate lower and upper bounds for the bearing capacity of a single, vertical and free-headed laterally loaded pile foundation, resting on a cohesive-frictional soil are calculated rigorously using finite elements and nonlinear programming via Optum^{G3}.

3.4 Finite element model:

The size of the soil domain is selected such that it contains the failure surface, Figure 5. Boundary effects are not expected on the calculated load, displacements or soil deformation mechanisms, which was also verified by conducting analyses with larger soil domains. The vertical sides of the soil domain are restrained from any lateral displacement whereas the bottom boundary is restrained from any vertical displacement. The top boundary is free to move. The side friction between pile and soil is modelled by using interface/shear joint elements at the pile soil boundary with same characteristics as the soil (i.e.: strength reduction factor =1) to ensure that the solution is a true upper bound. The gap formation at the back of the pile is thus allowed. The lateral loading consists of horizontal load and bending moment at pile head.

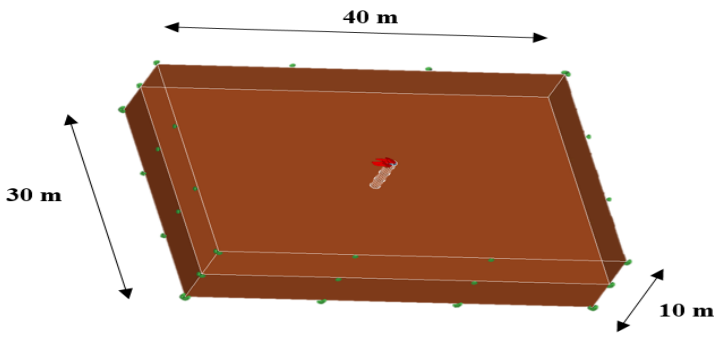

Figure 5. Finite element model dimensions

The mesh adaptivity option is used with the shear dissipation as the adaptive control parameter, Figure 6. The results of mesh sensitivity study are shown in Figure 7.

$$\text{Error}\ (\%) = \frac{UB - LB}{UB + LB} \times 100 \tag{3}$$

The worst case error, defined in Equation 3 is plotted as a function of the number of elements. As expected, the number of elements improves the accuracy of the finite element computations. For time computing reasons, a total number of 15 000 elements is adopted in all the simulations.

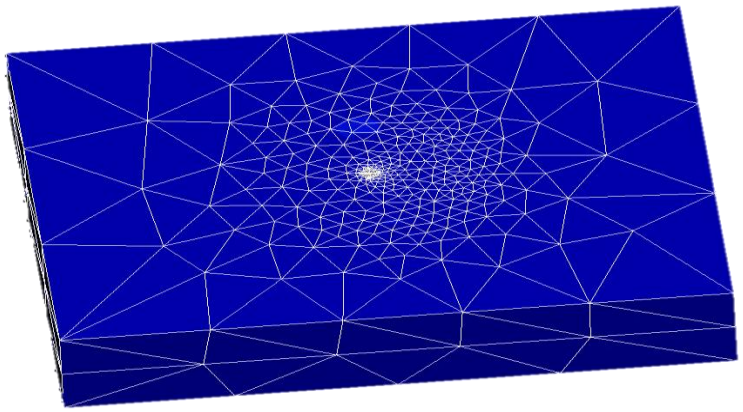

Figure 6. Adaptive mesh

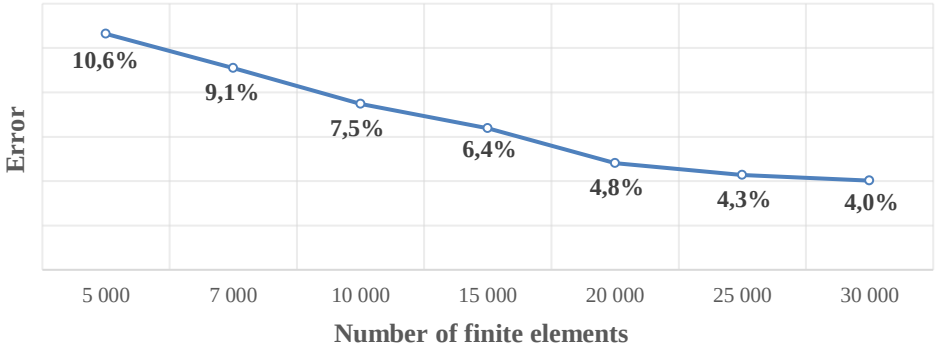

Figure 7. Mesh sensitivity study

4. FAILURE SURFACE IN THE M-H SPACE

The rigid pile is subjected to a combined static loads of overturning moment and horizontal force under a constant *M*/*H* ratio: radial paths in *M*-*H* plane, Figure 8. Taking advantage of the symmetry of the problem, only the first and the fourth quadrants of the failure surface in the loading space of the horizontal pile head load and moment are investigated (α ranging from -90° to 90°).

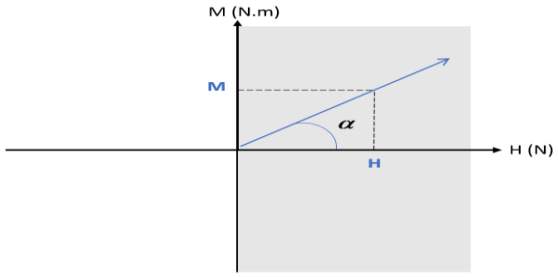

Figure 8. Radial paths in M-H load plane

The failure mode of a short rigid pile consists of rigid body rotation about a point located below ground surface, close to its toe and estimated at approximately 0.7 times its embedment length as measured from the ground surface. In fact, as the lateral earth pressures reach the ultimate passive lateral resistance of the soil along the pile length, the pile rotates around a point somewhere along its length and causes the development of a passive resistance in the soil in front of the pile above the rotation point and in the back side of the pile below the rotation point. Once the mobilizing passive resistance is equal to the limit state of the passive earth pressure, failure takes place. This failure mechanism is depicted in Figure 9, representing shear dissipation zone in the soil.

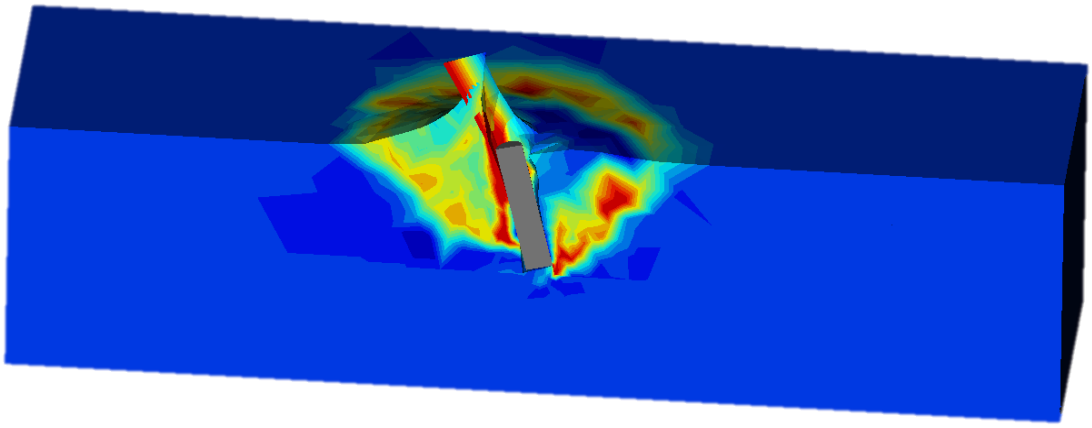

Figure 9. Shear dissipation in the soil mass

A large number of numerical radial tests are performed and the resulting bounds of the failure surface are plotted in Figure 10. The worst case error, ranges from 3.8 % to 6.4 % for this simulation and generally from 3% to 10% in all the cases simulated.

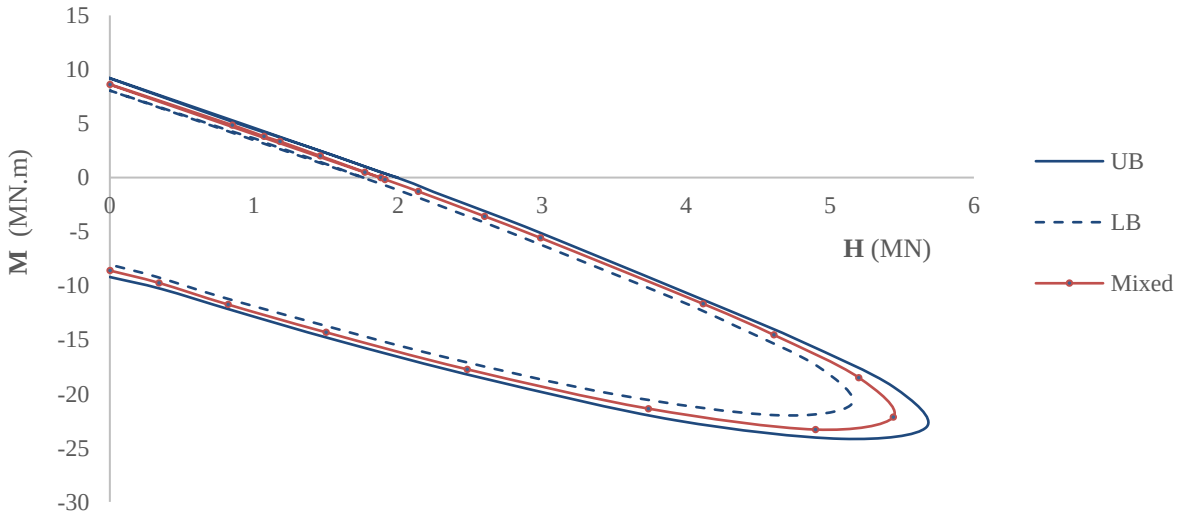

Figure 10. Upper and lower bounds for the failure surface in *M-H* plane.

The failure envelope present a distinguishable tilted elliptical shape. This format can be understood by analysing the loading direction of both the horizontal load and bending moment. The respective signs of both *H* and *M* has a substantial evident influence on the horizontal bearing capacity of the pile. In fact, in the first quadrant, which corresponds to same lateral loading directions ($HM > 0$), the presence of the overturning moment accelerates the failure of the pile soil system and hence the horizontal bearing

capacity is reduced. The curve is almost linearly decreasing in this part. Nonetheless, in the fourth quadrant corresponding to an opposite loading direction ($HM < 0$), the horizontal bearing capacity is at first increasing then decreasing. The maximum moment the pile can sustain did not occur when $H = 0$ but when there is a combination of positive horizontal load and negative bending moment. This can be explained by the fact that pile motion due to horizontal forces only are counterbalanced by motion in opposite direction due to bending moment. At a certain level, a greater moment is required to overcome the horizontal force and so higher values of moment are attained. The extrapolated mean of the upper and the lower bounds to the failure surface is presented normalized with respect to the pure moment M_0 and horizontal load H_0 in Figure 11.

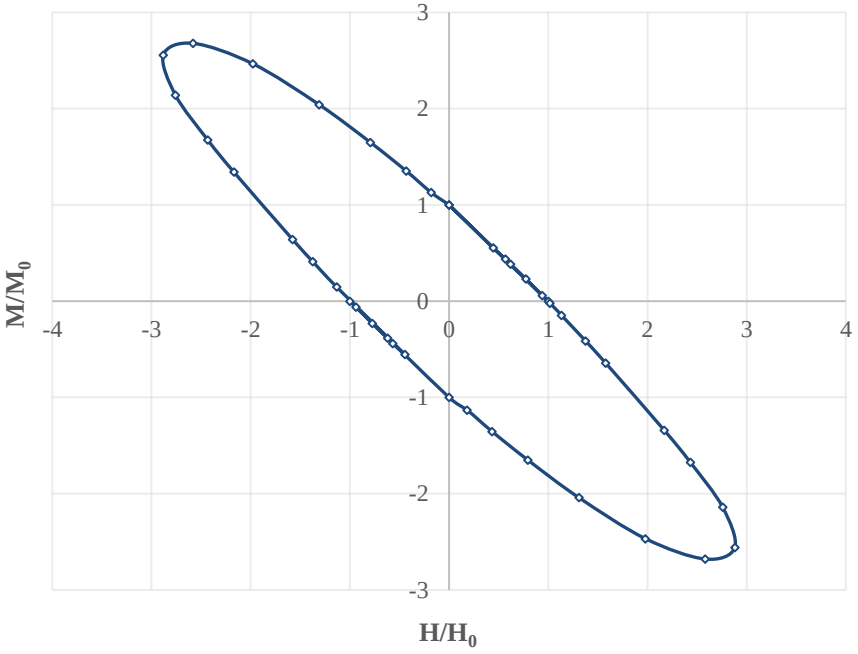

Figure 11. Estimated failure surface in M/M_0. H/H_0 plane.

Another alternative to rigorous upper and lower bounds is the mixed element solution which involves both variables velocities and stresses and provides a solution that generally lies between the upper and lower bound, see Figure 10. In all the cases simulated, the failure surface resulting from the mixed approach lies perfectly in between the upper and lower bounds relative to the same case.
The numerical results from both the upper and lower bounds were used to construct the failure surface. As discussed, the shape of the failure surface is a rotated ellipse whose parameters have been computed using a MATLAB script which enables to find the best fit to an ellipse for a given set of points using least squares criterion. Starting from the canonical representation of an ellipse, recalled in Equation 4, the coefficients A, B, C, D, E and F were determined for each numerical simulation.

$$f(\boldsymbol{H},\boldsymbol{M}) = A\left(\frac{H}{H_0}\right)^2 + B\left(\frac{H}{H_0}\right)\left(\frac{M}{M_0}\right) + C\left(\frac{M}{M_0}\right)^2 + D\left(\frac{H}{H_0}\right) + E\left(\frac{M}{M_0}\right) + F = 0 \quad (4)$$

Figure 12 shows the fitted ellipse to the upper and lower bounds to the normalized failure surface respectively. Perfect fit is observed globally with less accuracy at the extremities in case of upper bound. More details regarding the coefficients values will be given in the next section.
To visualize the influence of soil internal friction angle, cohesion, as well as unit weight and the pile geometry through pile length to diameter ratio on the shape of the failure surface, additional parametric numerical limit analysis simulations were conducted. The next section presents the main results.

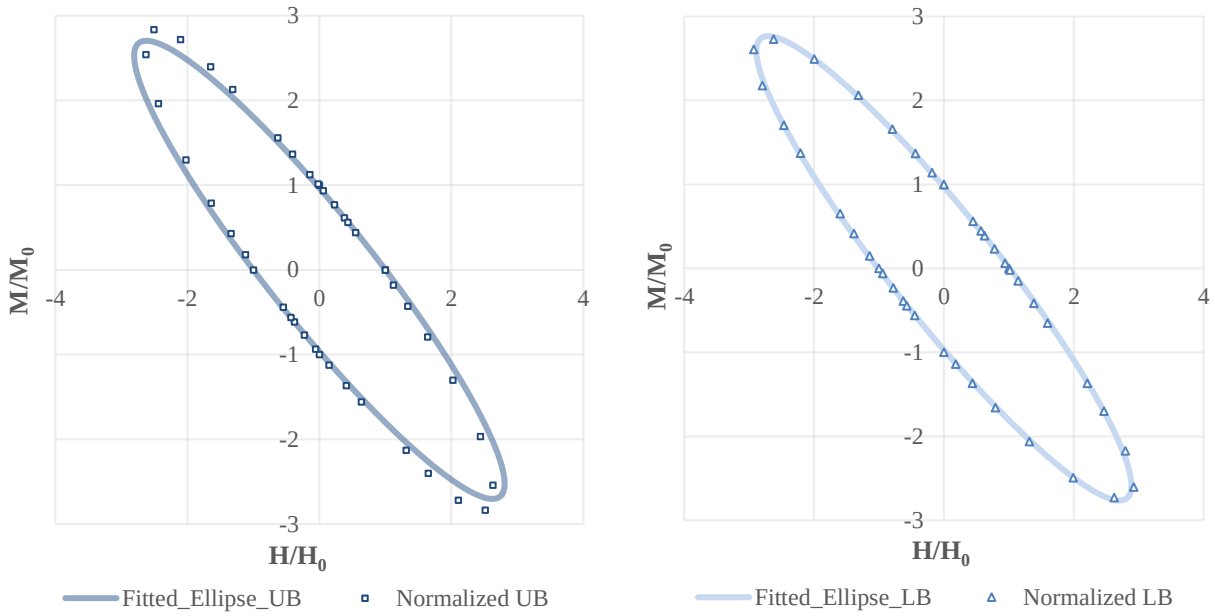

Figure 12. Ellipse fitting to failure surface Upper and Lower bounds

5. EFFECTS OF SOIL PROPERTIES AND PILE GEOMETRY

5.1 Effect of soil parameters

Soil friction angle (φ) is a major shear strength parameter. To investigate its effect on the shape of the elliptical failure surface, a parametric study is conducted with φ equal to 20°, 30° and 45°. Figure 13a presents the resulting upper and lower bounds in non-normalized form whereas Figure 13b presents the estimated failure surface (mean of UB and LB) for each case. As expected, the lateral loading capacity as well as the extent and depth of the plastic zone increases considerably with higher soil friction angle. It's also worth noting that the accuracy of the upper and lower bounds decreases as the friction angle increases with an average discrepancy of 4.8% for $\varphi = 20°$ to 9.4% for $\varphi = 45°$.

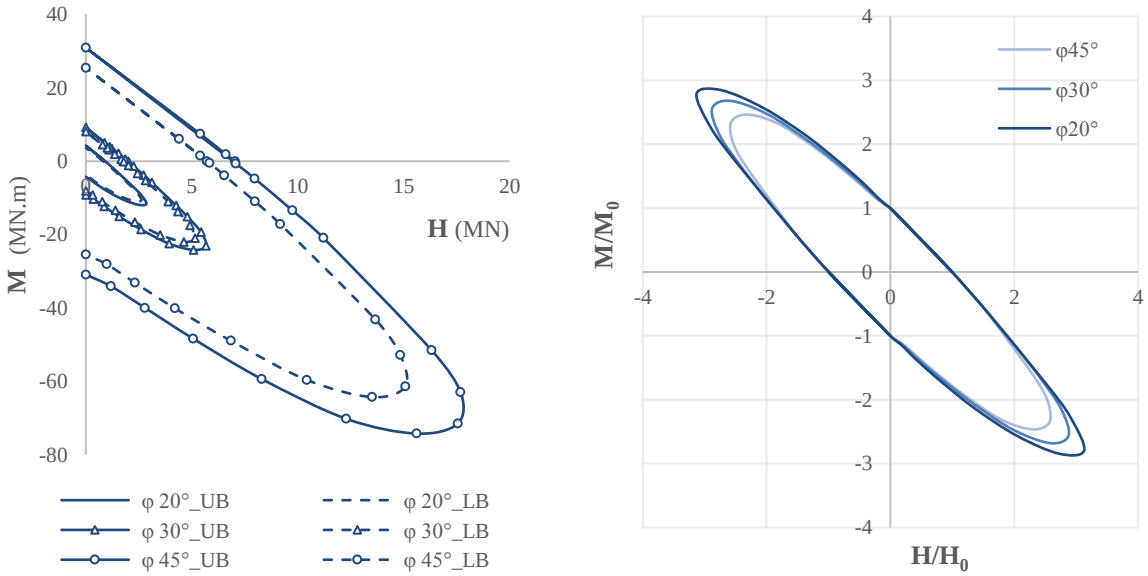

Figure 13. Effect of internal friction angle on the shape of the failure surface (a) *M-H* plane (b) M/M_0 - H/H_0 plane

While the ellipse centre coordinates are almost coincident with the origin ($X = 0, Y = 0$), the rotation angle and semi-minor axis remain quasi-constant, the semi-major axis of the normalized elliptical failure surface is decreasing with increasing value of φ. Similarly, soil cohesion is varied from 0, 10 to 50 kN/m^2. Results are shown in Figure 14. The normalized failure surface expands as the cohesion decreases. Soil friction angle and cohesion are the main strength parameters of the embedding soil. Higher values of c and φ reflects a stronger soil capable of withstanding higher lateral loads and consequently with higher bearing lateral capacity.

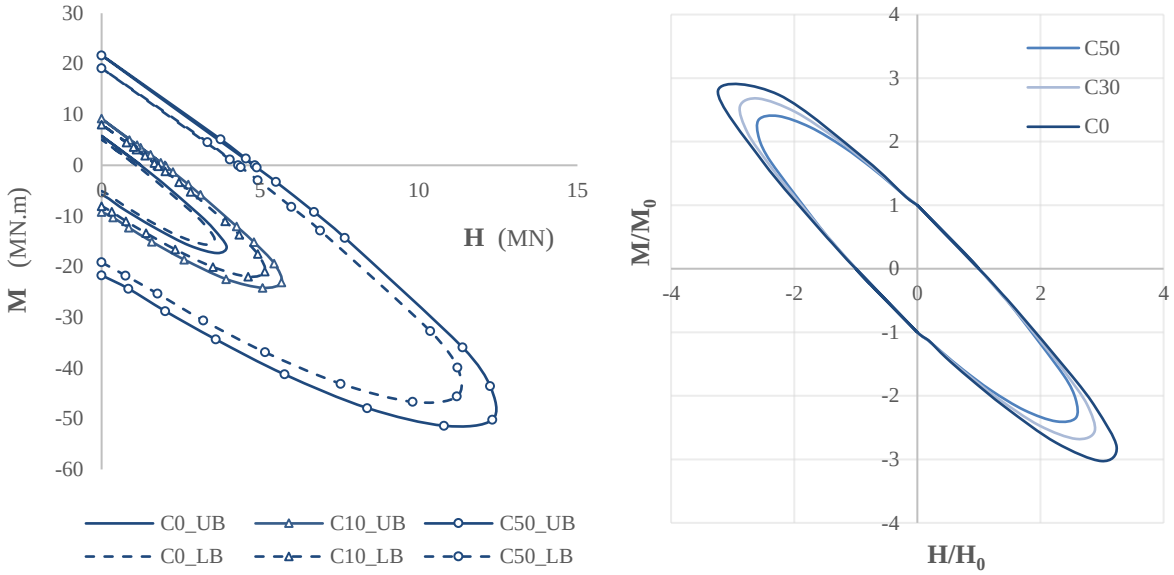

Figure 14. Effect of soil cohesion on the shape of the failure surface (a) *M-H* plane (b) M/M_0 - H/H_0-plane

The upper and lower bounds to the failure surface were computed for two different values of soil unit weight $\gamma = 20\ kN/m^3$ and $\gamma = 30\ kN/m^3$. Comparison is presented in Figure 15.

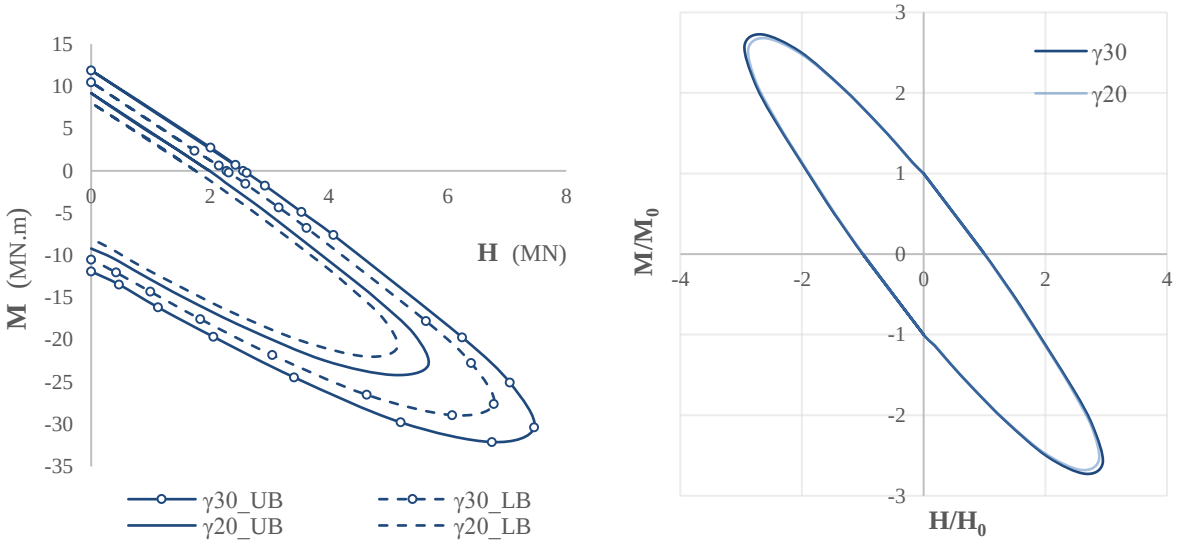

Figure 15. Effect of soil unit weight on the shape of the failure surface (a) *M-H* plane (b) M/M_0 - H/H_0-plane

5.2 Effect of pile aspect ratio

Pile geometry, particularly pile embedment length L to pile diameter D ratio, is one of the dominant factors affecting the lateral load and moment carrying capacity of short single piles. The pile geometry

used in previous numerical simulations is 5 ($L = 5\ m,\ D = 1m$). Comparison with both embedment ratios of 3 and 2 is investigated. As seen in Figure 16, the lateral load and moment carrying capacities of short single piles increases with increasing pile embedment ratio (L/D).

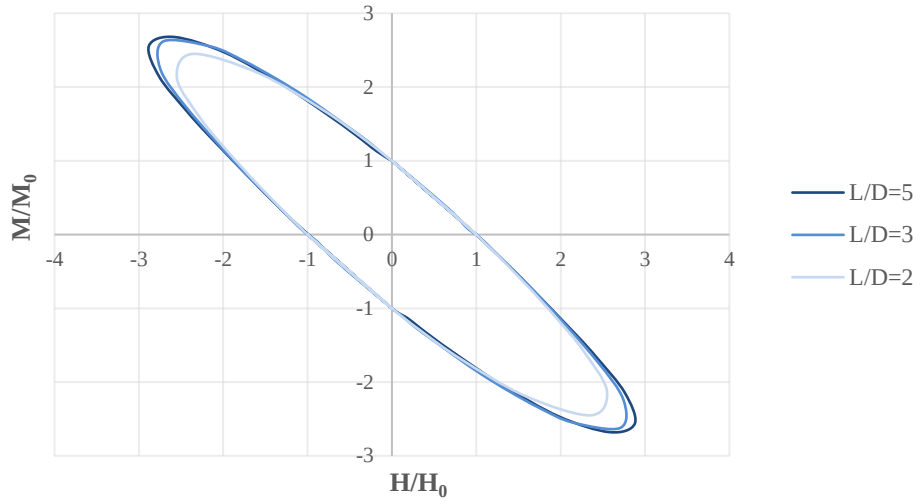

Figure 16. Effect of pile length to diameter ratio on the shape of normalized failure surface in M/M_0 - H/H_0-plane

5.3 Closed form expression

The coefficients A, B, C, D, E and F of Equation 4 are approximated for all the cases investigated, results are presented in Table 2 for the estimated failure surface (mean of UB, LB). In fact, the analytical expression that best fits the data, can be approximated to the form in Equation 5, with $A = C \approx 1$ and $D = E \approx 0$ (ellipse centred at the origin) while $F = -1$.

$$f(\boldsymbol{H},\boldsymbol{M}) = \left(\frac{H}{H_0}\right)^2 + B\left(\frac{H}{H_0}\right)\left(\frac{M}{M_0}\right) + \left(\frac{M}{M_0}\right)^2 - 1 \qquad (5)$$

B is the coefficient that controls the expansion of the failure surface in normalized M/M_0 - H/H_0 plane. Assuming it is a function of only c, φ, γ and L/D, regression analysis resulted in the following expression for B:

$$B = 0{,}0273 \cdot \tan(\boldsymbol{\varphi}) - 0{,}1581 \cdot \left(\frac{\boldsymbol{L}}{\boldsymbol{D}}\right)^{0{,}3258} + 8{,}6680 \cdot \left(\frac{\boldsymbol{c}}{\boldsymbol{L\gamma}}\right)^{8{,}035} - 1{,}6547 \qquad (6)$$

However, other parameters like soil pile interface conditions have without doubt a considerable impact on the pile lateral load capacity and should be accounted for.

Table 2. Fitted Ellipse Coefficients.

Ellipse coeff.	**φ=45°**	**φ=30°**						**φ=20°**	***Mean***
	c=10	**c=50**	**c=10**				**c=0**	**c=10**	
	γ=20			**γ=30**	**γ=20**				
	L/D=5				**L/D=3**	**L/D=2**	**L/D=5**		
A	0,9973	0,9800	0,9918	0,978036	0,9659	0,9700	0,9779	0,9841	*0,9810*
B	**-1,8983**	**-1,8779**	**-1,9250**	**-1,908370**	**-1,8390**	**-1,8374**	**-1,9298**	**-1,9108**	***-1,8883***
C	1,0630	1,0634	1,0661	1,058227	1,0141	1,0366	1,0555	1,0407	*1,0485*
D	0,0000	0,0071	0,0074	0,000000	0,0000	0,0000	0,0242	0,0000	*0,0055*

E	0,0000	-0,0070	-0,0074	0,000000	0,0000	0,0000	-0,0237	0,0000	*-0,0054*
F	-1	-1	-1	-1	-1	-1	-1	-1	*-1*

6. CONCLUSIONS

The simplicity, time efficiency and accuracy of the macro element approach makes it a very practical and competitive design tool for simulating the non-linear SSI effects in a seismic analysis of a superstructure. This paper presents a key step in the development of a novel pile head macro-element, within the elastoplastic framework, which is the investigation of the yield surface in horizontal and moment loading space. Numerical limit analysis approach is adopted. Both lower and upper bound to the limit load are accurately computed via the powerful 3D limit analysis code OPTUM^{G3}. The failure surface of a single, vertical, circular, free-headed and rigid pile embedded in a Mohr-Coulomb soil is bracketed from above and below with a worst case error ranging from 3% to 10%. The failure surface is fitted to a rotated ellipse equation and the influence of soil friction angle, cohesion and unit weight as well as pile length to diameter ratio on the shape of the bearing strength surface is discussed. These three parameters have a direct effect on the semi-major axis of the ellipse and so its expansion. An analytical expression is proposed additionally. Complementary and more in depth parametric studies based on dimensionless parameters will be conducted in future studies. Comparison and validation with results from the literature will be also carried out.

7. ACKNOWLEDGMENTS

This project has received funding from the European Union's Horizon 2020 research and innovation program under the Marie Skłodowska-Curie grant agreement no. 721816.

8. REFERENCES

Correia A. A., Pecker A., Kramer S.L., Pinho R. (2012). Nonlinear pile-head macro-element model: SSI effects on the seismic response of a monoshaft-supported. *Proceedings of the 15th World Conference on Earthquake Engineering*, Lisbon, Portugal, Paper No. 5527

Ertugrul T., Rha C., and Wallace J.W. (2006). A Robust Macroelement Model for Soil–Pile Interaction under Cyclic Loads. *Journal of Geotechnical and Geoenvironmental Engineering*, 132(10):1304–14.

Finn W. D. L. (2005), A study of piles during earthquakes: Issues of design and analysis. *Bulletin of Earthquake Engineering*, Vol 3, p. 141-234

Krabbenhoft K., Lyamin A., Krabbenhoft J. Optum computational engineering (OptumCE). 2015. Available on:<www.optumce.com>.

Li Z., Kotronis P., Escoffier S., Tamagnini C. (2016). A hypoplastic macroelement for single vertical piles in sand subject to three-dimensional loading conditions, *Acta Geotechnica*, Springer Verlag, 2016, 11 (2), pp.373-390

Lyamin A.V. and Sloan S.W. (2001). Upper Bound Limit Analysis Using Linear Finite Elements and Non-Linear Programming. *International Journal for Numerical and Analytical Methods in Geomechanics*, 26(2):181–216.

Lyamin A.V. and Sloan S.W. (2002). Lower bound limit analysis using non-linear programming. *International Journal for Numerical Methods in Engineering* , 55(5):573–611.

Pecker A. (2015) Seismic Analyses and Design of Foundation Soil Structure Interaction. In: Ansal A. (eds) Perspectives on European Earthquake Engineering and Seismology. *Geotechnical, Geological and Earthquake Engineering* 39, Springer, Cham, pp:153–62.